Research Article | Vol. 33, No. 20 / 6 Oct 2025 / Optics Express 43026
Optics EXPRESS

Single laser dual optical frequency comb generation

MARKO M. KRSTIĆ,[1,*] AMOL DELMADE,[2,3] JASNA V. CRNJANSKI,[1] LIAM BARRY,[2] AND DEJAN M. GVOZDIĆ[1]

[1] University of Belgrade, School of Electrical Engineering, Bulevar kralja Aleksandra 73, 11120 Belgrade, Serbia
[2] Radio and Optical Communication Lab, School of Electronic Engineering, Dublin City University, Dublin, Ireland
[3] Currently with Pilot Photonics Ltd, DCU Alpha, Glasnevin, Dublin 11, D11 P22X, Ireland
[*] marko.krstic@etf.bg.ac.rs

Abstract: In this paper we present a simple scheme of dual frequency comb generation, based on a large-signal electrical modulation of a single high-speed semiconductor laser, applicable for symmetric spectroscopic system architectures. Our simulation results, based on a detailed numerical model including parasitic and noise effects, are confirmed through an experiment, reporting almost 40 GHz wide dual optical frequency comb, with 160 beat notes of 10 MHz spacing.

1. Introduction

Optical frequency combs (OFCs), representing a spectrum composed of equally spaced and phase coherent optical lines have enabled breakthroughs in various fields of applications such as timekeeping [1], high-speed and high-capacity optical communications [2,3], broadband molecular spectroscopy [4,5], and particularly rxsevolutionized the field of precision metrology and RF photonics by providing a direct link between optical and radio frequencies [6,7]. Among the various implementations of frequency comb technology, dual frequency combs (DFCs) have emerged as a particularly powerful tool for high-resolution, broadband, and rapid, real-time measurements without moving parts [8–10].

A usual DFC system utilizes two optical frequency combs with slightly different repetition rates. When these combs are heterodyned on a photodetector, they generate a series of RF beat notes that directly map the optical domain into the RF domain. The required condition is that these two combs are mutually coherent, which is typically guaranteed by phase-locking of the two combs [9–11]. In the spectroscopic applications, two different DFC system architectures are used [8]. In the "asymmetric" architecture, the two combs undergo different paths, one passing through the sample, and then heterodyned with the other comb undergoing a free path, providing full phase and amplitude response of the sample [8]. In the other, "symmetric" or "common-path" technique both combs are passed through the sample and it stands for a simple, low-cost, and flexible architecture, more robust to turbulent measurement paths, although providing only the amplitude response of the sample [8,12]. However, a recent work [13] reports a symmetric DFC architecture upgrade, by presenting an algorithm capable of extracting spectral phase information.

Some of the state-of-the-art techniques for comb generation include femtosecond erbium-doped fiber lasers [9,14], various designs of mode-locked lasers [15,16], quantum cascade lasers [17], microresonators [18,19], and schemes utilizing electro-optic (EO) modulators [9,20]. Optical comb generation using the gain switching technique, although suffering from limitations in terms of high comb bandwidths, number of lines, and free spectral range, introduces scheme simplicity,

#575910 https://doi.org/10.1364/OE.575910
Journal © 2025 Received 8 Aug 2025; accepted 4 Sep 2025; published 30 Sep 2025

Optics EXPRESS

low power/energy footprint, free spectral range tunability, and possibility for photonic integration [21–23]. Current research efforts are indeed aimed towards such architectures, especially having in mind applications such as community-based sensing or distributed sensing networks where the cost, size, and complexity of the optical components are recognized as key factors [24]. Several DFC system realizations, based on the coupling of mutually injection-locked gain-switched lasers have been proposed [25–28]. However, schemes in [25,26] comprise an additional acousto-optic modulator, making them difficult for photonic integration, whereas [28] presents fully integrated solutions. In the case of an integrated solution [28], the device requires two lasers and the optical bandwidth of the DFC is around 25 GHz, however, comprising just five pairs of comb lines. The optical bandwidth of solutions involving acousto-optic modulators are higher, reporting 35 GHz optical bandwidth with 300 RF converted beat notes in 10 dB margin, with low RF powers in order of −100 dBm [26] and 100 beat notes in 20 dB RF power margin, ranging from around −30 dB to −50 dBm [25]. Finally [27], reports mutually injection-locked 2 μm wavelength laser system without additional modulators to obtain 49 beat notes in 30 dB RF power margin, ranging from around −50 dBm to −80 dBm. Recently, a new trend of a single laser cavity DFC is investigated, providing better mutual coherence of comb lines and common mode noise cancellation, with various methods of generation involved, such as wavelength-multiplexing, polarization-multiplexing, circulation-direction-multiplexing, and cavity-space-multiplexing, all applied to different mode-locked architectures [16], or using pulse-modulated laser and generation of two orthogonally polarized optical frequency combs, by leveraging the birefringence in the fiber resonator [29], or by means of dual wavelength mode-locked fiber lasers undergoing optimally designed spectral filtering [30]. Obtainable line separation and heterodyne frequencies range from several MHz to tens of GHz, and several Hz to hundreds of MHz, respectively [16], and are used within specific spectroscopic applications. However, it has been reported that DFCs with GHz line separation can provide a better trade-off between spectral resolution and refresh rate for measuring sparse events [30], and such combs have been used paired with both kHz [16] and MHz heterodyne frequencies [31].

In this paper, we present a simple, compact, low-power scheme for DFC generation, applicable in the symmetric spectroscopic system architecture [8,12]. Our technique is based on a large-signal electrical modulation of a single high-speed DFB laser, and we report experimentally obtained 40 GHz optical bandwidth DFC, with 160 resolved, 10 MHz spaced RF beat tones in around 30 dB power margin. The paper is organized as follows. Section 2 presents the theoretical model of the modulated DFB laser, taking into account parasitic and noise effects. In Section 3 we present the experimental setup used to record theoretically predicted DFC, while in Section 4 we outline and discuss obtained results before presenting conclusions in Section 5.

2. Theoretical model

In order to fully describe the dynamics of the laser diode in the regime of large signal modulation, we employ an extended rate equation model that accounts for carrier transport and parasitic effects, similar to the model in [32,33]. As opposed to [32,33], where we neglect the noise terms, in this work we include stochastic terms in order to provide a more sophisticated model, able to predict the temporal response of the laser diode and consequently the shaping of the comb lines more realistically. The model describes the dynamics of a multiple quantum well DFB laser and comprises of four stochastic differential equations following the dynamics of the carrier density in the barrier states (n_b), carrier density in the bound states of the well region (n_w), photon density

Optics EXPRESS

(S) and the evolution of the optical phase (φ), and is written in the matrix form as:

$$\mathrm{d}\begin{bmatrix} n_\mathrm{b} \\ n_\mathrm{w} \\ S \\ \varphi \end{bmatrix} = \begin{bmatrix} \eta_\mathrm{inj} I (q V_\mathrm{tot})^{-1} - n_\mathrm{b}\tau_\mathrm{b}^{-1} - n_\mathrm{b}\tau_\mathrm{bw}^{-1} + n_\mathrm{w} V_\mathrm{w} (\tau_\mathrm{wb} V_\mathrm{tot})^{-1} \\ n_\mathrm{b} V_\mathrm{tot} (\tau_\mathrm{bw} V_\mathrm{w})^{-1} - n_\mathrm{w}\tau_\mathrm{w}^{-1} - n_\mathrm{w}\tau_\mathrm{wb}^{-1} - v_\mathrm{g}\Omega(n_\mathrm{w} - n_0) S(1+\varepsilon S)^{-1} \\ \Gamma v_\mathrm{g}\Omega(n_\mathrm{w} - n_0) S(1+\varepsilon S)^{-1} - S\tau_\mathrm{p}^{-1} + \Gamma\beta_\mathrm{sp} R_\mathrm{sp}(n_\mathrm{w}) \\ 0.5\alpha \left(\Gamma v_\mathrm{g}\Omega(n_\mathrm{w} - n_0)(1+\varepsilon S)^{-1} - \tau_\mathrm{p}^{-1}\right) \end{bmatrix} \mathrm{d}t + \boldsymbol{F}\mathrm{d}\boldsymbol{W}. \quad (1)$$

Here, $\boldsymbol{F}$ is a 4×4 operator comprising the noise coefficients F_{ij} ($i,j \in \{n_\mathrm{b}, n_\mathrm{w}, S, \varphi\}$) and $\mathrm{d}\boldsymbol{W}$ is the column vector of noise realizations given as $[G_{n_\mathrm{b}}(0,1)\ \ G_{n_\mathrm{w}}(0,1)\ \ G_S(0,1)\ \ G_\varphi(0,1)]^\mathrm{T}\mathrm{d}\sqrt{t}$, where $G_i(0,1)$ stands for independent Gaussian processes with zero mean and unit variance [34,35].

The deterministic model parameters are fitted to the Gooch & Housego AA0701 series, 1.55 μm high modulation bandwidth DFB laser diode as in [33]. An exception with respect to [32,33] is in the definition of the total spontaneous emission rate R_sp which is here taken more rigorously, due to it's crucial impact on the noise. In this work, we adopt functional dependence of $R_\mathrm{sp}(n_\mathrm{w})$ on the carrier concentration in the well region, calculated for a multi-quantum well, strain-compensated high-speed laser, as in [36]. The description of the deterministic parameters and their values is given in Table 1.

Table 1. Laser parameters used in the simulation

Symbol	Definition	Value
η_inj	injection efficiency	0.85
V_tot	total volume of the laser	1.03×10^{-10} cm^{-3}
V_w	volume of the wells	1.68×10^{-11} cm^{-3}
τ_b	carrier recombination lifetime in the barrier	2.5 ns
τ_w	carrier recombination lifetime in the well	1.5 ns
τ_bw	carrier capture time	14.5 ps
τ_wb	carrier escape time	70 ps
v_g	group velocity of the light	8.5×10^9 cm/s
Ω	differential gain	1.5×10^{-15} cm^2
Γ	optical confinement factor	0.08
n_0	carrier transparency concentration	4.2×10^{18} cm^{-3}
τ_p	photon lifetime	2.3 ps
ε	nonlinear gain suppression coefficient	2×10^{-17} cm^3
α	linewidth enhancement factor	3.5
β_sp	spontaneous emission coupling factor	7×10^{-6}
$R_\mathrm{sp}(n_\mathrm{w})$	total spontaneous recombination rate	calculated in [36]
η_0	optical efficiency	0.15
ω_0	lasing angular frequency	$2\pi \times 194.5371$ THz

Langevin noise coefficients F_{ij} are equal to the square root of the corresponding correlation strength D_{ij}, i.e., $F_{ij} = \pm\sqrt{D_{ij}}$, where cross-correlations ($i \neq j$) are taken to be negative [34,35]. Correlation strengths are derived by following the approach given in [34], assuming that the laser noise originates from shot noise associated with the discrete random flow of particles into and

Optics EXPRESS

out of the reservoirs of carriers (both in the barrier and well regions) and photons:

$$D_{n_\mathrm{b},n_\mathrm{b}} = \frac{\eta_\mathrm{inj} I(t)}{q V_\mathrm{tot}^2} + \frac{n_\mathrm{b}}{\tau_\mathrm{b} V_\mathrm{tot}} + \frac{n_\mathrm{b}}{\tau_\mathrm{bw} V_\mathrm{tot}} + \frac{n_\mathrm{w} V_\mathrm{w}}{\tau_\mathrm{wb} V_\mathrm{tot}^2}, \tag{2a}$$

$$D_{n_\mathrm{w},n_\mathrm{w}} = \frac{n_\mathrm{w}}{\tau_\mathrm{w} V_\mathrm{w}} + 2\Gamma\beta_\mathrm{sp} R_\mathrm{sp}(n_\mathrm{w}) S - \frac{v_\mathrm{g}\Omega(n_\mathrm{w}-n_0)}{V_\mathrm{w}(1+\varepsilon S)} S + \frac{n_\mathrm{b} V_\mathrm{tot}}{\tau_\mathrm{bw} V_\mathrm{w}^2} + \frac{n_\mathrm{w}}{\tau_\mathrm{wb} V_\mathrm{w}}, \tag{2b}$$

$$D_{S,S} = 2\Gamma\beta_\mathrm{sp} R_\mathrm{sp}(n_\mathrm{w}) S, \tag{2c}$$

$$D_{\varphi,\varphi} = \frac{\Gamma\beta_\mathrm{sp} R_\mathrm{sp}(n_\mathrm{w})}{2S}, \tag{2d}$$

$$D_{n_\mathrm{b},n_\mathrm{w}} = D_{n_\mathrm{w},n_\mathrm{b}} = \frac{n_\mathrm{b}}{\tau_\mathrm{bw} V_\mathrm{w}} + \frac{n_\mathrm{w}}{\tau_\mathrm{wb} V_\mathrm{tot}}, \tag{2e}$$

$$D_{n_\mathrm{w},S} = D_{S,n_\mathrm{w}} = 2\beta_\mathrm{sp} R_\mathrm{sp}(n_\mathrm{w}) S - \frac{\Gamma v_\mathrm{g}\Omega(n_\mathrm{w}-n_0)}{V_\mathrm{w}(1+\varepsilon S)} S, \tag{2f}$$

$$D_{n_\mathrm{w},\varphi} = D_{\varphi,n_\mathrm{w}} = D_{n_\mathrm{b},\varphi} = D_{\varphi,n_\mathrm{b}} = D_{n_\mathrm{b},S} = D_{S,n_\mathrm{b}} = D_{\varphi,S} = D_{S,\varphi} = 0. \tag{2g}$$

As in our previous work [32], the laser diode is driven by the electrical current $I(t)$ in the form which superimposes DC bias current (I_b) and large-signal modulation composed of the sum of two trains of *sinc*-shaped pulses with same amplitudes ΔI and close-valued modulation frequencies f_1 and $f_2 = f_1 + \delta f$, where $\delta f \ll f_1$:

$$I(t) = I_\mathrm{b} + h(t) \sum_{k=1}^{2} \Delta I \frac{\sin(2\pi N f_k t)}{N \sin(2\pi f_k t)}, \quad \text{with} \quad \lim_{t \to f_k^{-1}} \frac{\sin(2\pi N f_k t)}{N \sin(2\pi f_k t)} = 1. \tag{3}$$

In the equation above, $h(t)$ denotes the Heaviside step function, i.e., the modulation starts after the laser has stabilized its continuous wave output. Finally, parameter N defines the bandwidth of the applied electrical current. In this work we use odd values of N, for which the current waveform consists of positive current spikes [32]. The stochastic differential equations system (1)-(2) is numerically solved applying Euler-Maruyama method, with step size Δt sufficiently smaller than the fastest time scale, i.e., τ_p in this case, and the solution is averaged over multiple realizations of the system. The output optical frequency comb is obtained by taking the Fourier transform of the laser diode complex electrical field, expressed as $E(t) = \sqrt{S(t)} e^{-i\varphi(t)}$. The time window in which (1) is solved is taken with respect to the desired resolution of the Fourier transform, which should be smaller than δf. Finally, the output optical power P is converted from the photon density using $P(t) = \eta_0 V_\mathrm{w} \hbar\omega_0 S(t)/(\tau_\mathrm{p}\Gamma)$ [32], with η_0 and ω_0 given in Table 1.

3. Experimental setup

Figure 1 shows the experimental setup used for verifying the generation of the dual optical frequency comb. The *sinc*-shaped pulses, represented by Eq. 3, were generated offline in MATLAB, and the samples were loaded to the arbitrary waveform generator (AWG). The Keysight AWG, M8195A with a bandwidth of ≈23 GHz, was operated at a sampling rate of 60 GSa/s with an output signal swing of 500 mV (−2 dBm power). The dual *sinc* pulse signal with f_1 = 800 MHz and δf = 5 MHz (f_2 = 805 MHz) was generated offline over a repeating period of 200 ns for this demonstration. The generated signal was amplified using a 16 dB gain electrical RF amplifier to boost its power to the desired level. This signal was superimposed to the laser driver (LD) bias current I_b and used for the direct modulation of a temperature controlled (TEC) DFB laser with an internal bias tee and with 18 GHz of −3 dB bandwidth. A 50 : 50 splitter was used to send portions of the optical signal to the Apex Technologies optical spectrum analyzer (OSA) with a resolution of 5 MHz and photodiode (PD). Dual comb generated beatings, recorded

Optics EXPRESS

by the PD, were characterized by a 40 GHz bandwidth electrical spectrum analyzer (ESA) from Anritsu with 1 kHz resolution. The ESA was also used to characterize the dual *sinc* pulse signal generated by the AWG.

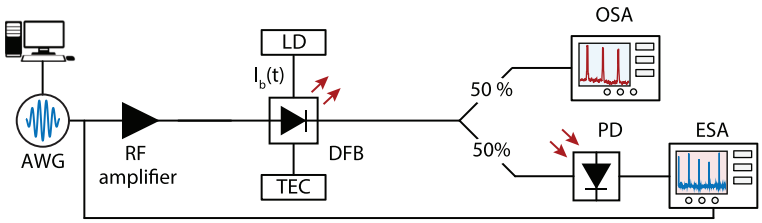

Fig. 1. Experimental setup for the generation of dual frequency comb based on direct modulation of a semiconductor laser.

4. Results and discussion

In Fig. 2(a) we show a simulated waveform of the used electrical driving current, given by Eq. (3), in three different time windows. The laser bias current I_b was kept at $5I_{th} = 55$ mA, giving ≈6 dBm output optical power from the DFB laser. The AWG signal was amplified to $\Delta I = 5.13I_{th}$. The figure illustrates the superposition of the two trains of *sinc*−shaped pulses which appear with repetition rates of $2f_1 = 1600$ MHz and $2f_2 = 1610$ MHz. By setting $N = 25$, the electrical current bandwidth of $N \times f_2 \approx 20$ GHz was set. Frequency offset between the train of pulses equal to $2\delta f = 10$ MHz defines that pulses from two trains completely overlap and add at each 100 ns (first time window in Fig. 2(a)). Between the two adjacent pulse overlappings, the pulses from the two trains spread and then come back together, with separation within the pulse pair increasing in the first (Fig. 2(b)), and deceasing in the second half of the 100 ns period (Fig. 2(c)). The corresponding signal spectrum, captured by the ESA is presented in Fig. 2(b), showing twelve pairs of dual *sinc* tones separated by 1.6 GHz, with separation within the pair increasing in multiples of 10 MHz as $n \times 10$ MHz, with n being the ordinal of the pair. The zoomed spectrum in the vicinity of 3.2 GHz tones (Fig. 2(c)) shows the second pair of tones ($n = 2$), with separation of 20 MHz.

In Fig. 3 we present a comparison between the simulated (blue line) and experimentally obtained (red line) DFC, showing excellent qualitative agreement. Simulation timestep for the model described with Eqs. (1)–(2) was approximately $0.12\tau_p$ and the solution was averaged over 10 realizations. In both cases the comb is structured as the series of pairs of comb lines, arranged on the both sides of the strong central comb line, originating from the fundamental lasing frequency (c.f. Figure 3(a)). Their optical power decreases more or less rapidly at the negative and positive spectrum side, respectively, for relative frequencies surpassing the modulation current bandwidth of 20 GHz, thus forming the 40 GHz optical DFC span. Although the theoretical model is nicely fitted to the laser used in the experiment, at least up to 25 GHz operation [33], the laser packaging induces strong decline of the bandwidth in the region of high frequencies, hence the simulated spectrum shows significantly stronger comb lines for the relative frequencies higher than |20 GHz|, in comparison to the experiment. Furthermore, the cumulative effect of the laser package parasitics and the modeled carrier transport, produces more noticeable frequency roll-off in the experiment in comparison with the simulation, leading to experimentally recorded spectrum with more pronounced dip in the region of ±10 GHz relative frequencies, as well as stronger lines in the vicinity of the central frequency. Finally, the simulated spectrum follows an experimentally visible slight increase in the comb envelope, in the vicinity of relative frequency ±16 GHz, which is theoretically calculated to correspond to the relaxation frequency for the given DC bias. For the sake of completeness, in Fig. 3(b) we

Optics EXPRESS

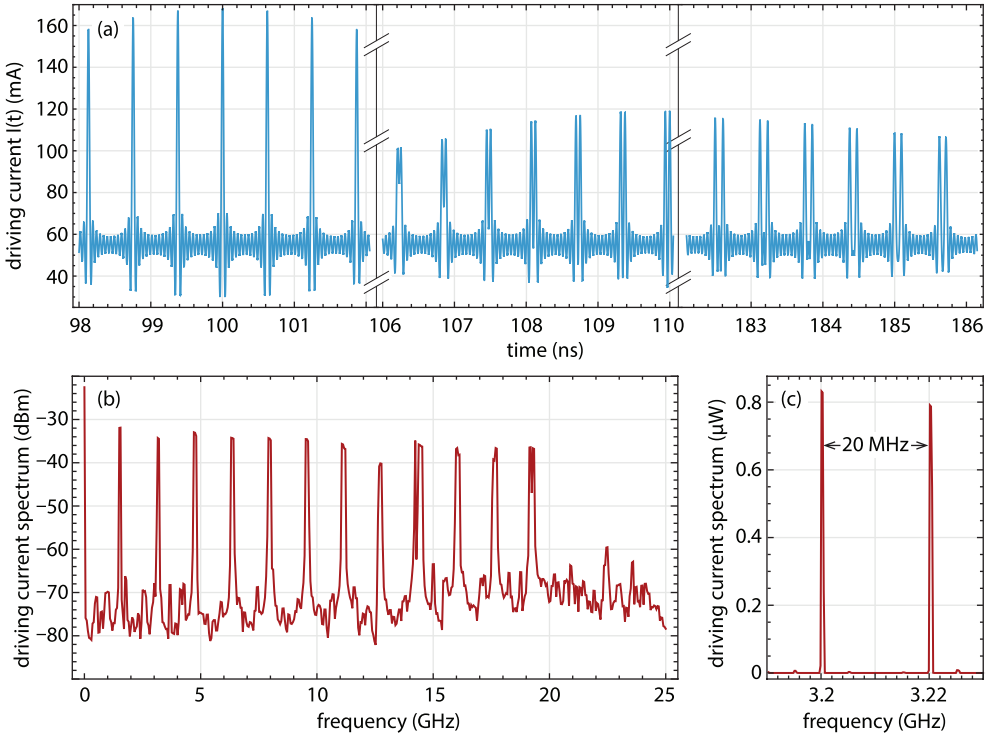

Fig. 2. (a) Simulated driving current waveform depicted in three different time windows. (b) Recorded electrical spectrum of the dual *sinc* pulse signal generated from AWG with (c) zoomed region around 3.2 GHz tones.

show experimentally recorded comb with respect to the actual optical power, which is in order of −40 dBm for comb lines within ±20 GHz relative frequency range. However, it should be noted that this is the 50% of the real optical power coming from the laser, due the 50:50 splitter used in the experiment (Fig. 1). In Fig. 3(c-d) we depict zooms of particular pairs of comb lines, comparing normalized simulation and experimental spectra (blue and red line, respectively), to verify that the arrangement of the lines as seen in the experiment, follows the prediction made by the model [32]. If we define the position of a pair of comb lines as the frequency in the middle of the pair, relative to the central comb line, then pairs of lines appear with frequency separation $\Delta f = f_1 + f_2 = 1600.5$ MHz, i.e., at relative frequencies $\pm n\Delta f$, with $n \in \mathbb{N}$ defined as the ordinal of the pair. With such frequency separation, in the ±20 GHz bandwidth we obtain $20/1.6005 \approx 12$ pairs of comb lines. The heterodyne frequency of a pair $\delta\nu_n$ increases with the ordinal number as $\delta\nu_n = n \times 2\delta f = n \times 10$ MHz. Indeed, Figs. 3(c-d) show zoomed pairs of lines for $n = 6$ and $n = 7$ with corresponding heterodyne frequencies of 60 and 70 MHz, respectively (Fig. 3(c)), and $n = 10$ and $n = 11$, with corresponding heterodyne frequencies of 100 and 110 MHz (Fig. 3(d)). The GHz/MHz ratio between separation f_1 and heterodyne δf frequencies has been chosen to ensure high number of beat notes, i.e., high bandwidth of the beating spectrum, while taking into account the aliasing limit [16]. However, in our case, the minimal heterodyne frequency is limited by the intrinsic laser linewidth, while the laser bandwidth affects the maximal frequency separation f_1. Nevertheless, within these constraints, other combinations of f_1 and δf are also possible. Moreover, applying injection-locking to the DFB laser under modulation could decrease the minimal heterodyne frequency even by an order of magnitude [37]. Finally, the linewidths of comb lines recorded in the experiment are higher in comparison with the ones

Optics EXPRESS

calculated theoretically, which is a consequence of low fundamental heterodyne frequency $\delta\nu_1$ of 10 MHz recorded with finite resolution optical spectrum analyzer, as well as the inability of the theoretical model to fully describe line broadening. However Figs. 3(c-d) show that measured results (red line) nicely envelope simulated results (blue line), especially in the region of noise induced broadening of the comb line pair.

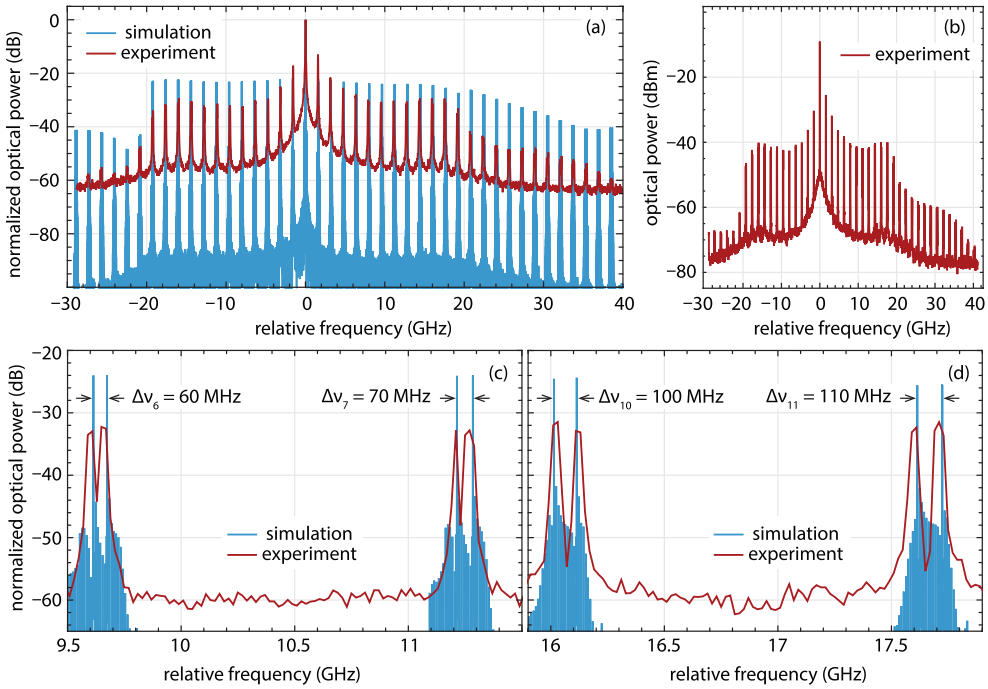

Fig. 3. (a) Normalized experimentally recorded (red line) and simulated (blue line) DFC. (b) Experimentally recorded optical power of the comb in units of dBm. Zoomed pair of lines with ordinal numbers $n = 6$ and $n = 7$ (c) and $n = 10$ and $n = 11$ (d) as predicted by simulation (blue line) and recorded in the experiment (red line).

In Fig. 4 we present an electrical spectrum of the presented DFC, recorded by high bandwidth photodetector and 1 kHz resolution electrical spectrum analyzer. Presented electrical spectrum exhibits a flat profile and follows the arrangement of the comb lines as predicted by theory, with rapid decrease in comb line power after surpassing the 20 GHz bandwidth.

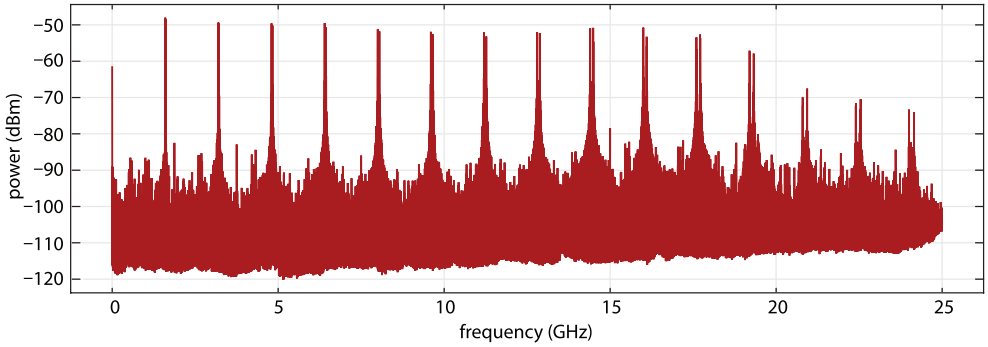

Fig. 4. Electrical spectrum of the DFC recorded with high bandwidth photodetector.

Optics EXPRESS

Finally, the RF beat spectrum is presented in Fig. 5, as recorded by small bandwidth photodetector and 1 kHz resolution electrical spectrum analyzer. As expected, the beating spectrum consists of lines at multiples of the 10 MHz fundamental heterodyne frequency. Although the optical spectrum exhibits a rapid power decrease after the 20 GHz bandwidth, i.e., consists of 12 strong pairs of comb lines at each side of the spectrum, the RF beat spectrum exhibits much wider span than 12 beat notes. In particular comb lines arrangement, considering pair separation of 1600 MHz and fundamental heterodyne frequency of 10 MHz, the spectrum would be limited to 160 comb line pairs on each spectrum side, before the heterodyne frequency of a particular pair overrides pair separation. Translated to the RF beat spectrum, it is worth considering beat notes up to 1600 MHz, which are all presented in Fig. 5(a), i.e., 160 RF beat notes, with RF power in around 30 dB margin. Figure 5(b-c) show two zoomed regions of the beating spectrum, clearly showing 10 MHz beat notes, albeit several artifacts appearing at irregular frequencies, however with significantly less power than the adjacent beat note, being stray signals picked up by the photodetector or the scope. The RF beat spectrum shows large power fluctuations which are mainly attributed to multiple RF signals being generated at each frequency with different relative phases, due to the nonlinear phase profile across the optical frequency comb lines. The non-ideal frequency response of the photodiode and RF amplifiers used can also introduce power fluctuations in the RF beat spectrum.

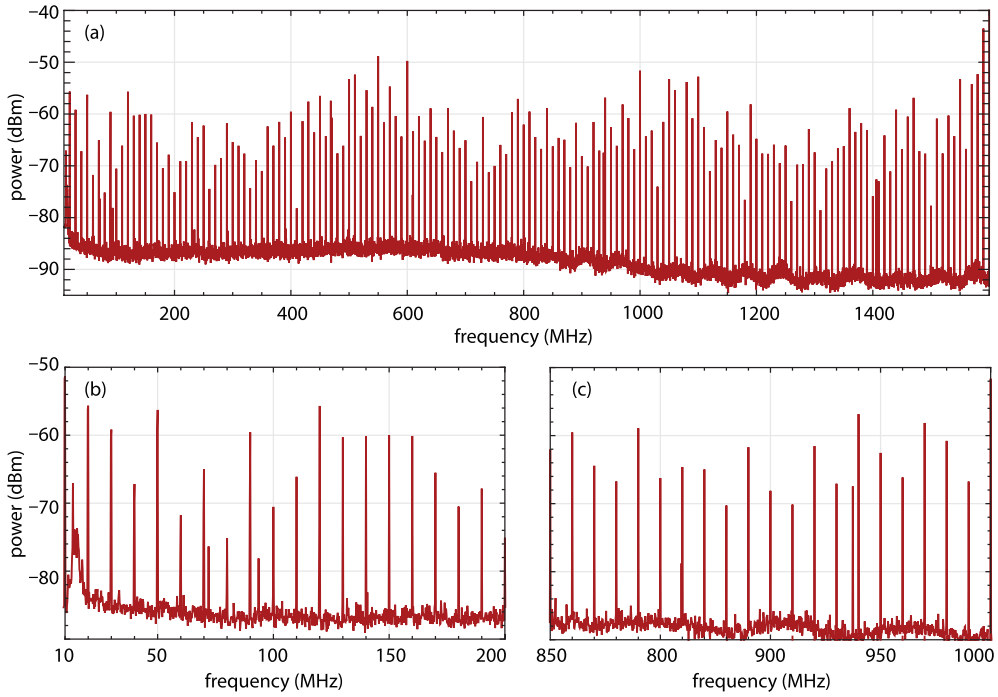

Fig. 5. (a) RF beat spectrum of the DFC showing 160 beat notes with 10 MHz free spectral. Zooms of the (b) 10 – 200 MHz and (c) 850 – 1000 MHz regions.

5. Conclusion

In this paper, a single high-speed semiconductor laser has been proposed for dual frequency comb generation. A simple technique based on large-signal electrical modulation, with tailored bias current waveform has been investigated by means of a detailed numerical model and experiment. Theoretical predictions have been confirmed by the experiment with good qualitative agreement,

Optics EXPRESS

and we report dual frequency comb with almost 40 GHz optical bandwidth, comprising of comb line pairs with 1600 MHz separation and heterodyne frequencies increasing in multiples of 10 MHz. In the RF domain, we report 160 beat notes with free spectral range equal to 10 MHz. To the best of our knowledge, this is the first experimental demonstration of dual frequency comb generated directly from a single laser.

Funding. Science Fund of the Republic of Serbia (6066816); Ministarstvo Prosvete, Nauke i Tehnološkog Razvoja (451-03-137/2025-03/200103); Science Foundation Ireland (13/RC/2077-P2, 12/RC/2276-P2); Palace of Science, Miodrag Kostić Endowment.

Disclosures. The authors declare no conflicts of interest.

Data availability. The datasets generated during and/or analyzed during the current study are available from the corresponding author on reasonable request.

References

1. L. Essen and J. V. L. Parry, "An atomic standard of frequency and time interval: A caesium resonator," Nature **176**(4476), 280–282 (1955).
2. H. Hu and L. K. Oxenløwe, "Chip-based optical frequency combs for high-capacity optical communications," Nanophotonics **10**(5), 1367–1385 (2021).
3. V. Torres-Company, J. Schröder, A. Fülöp, *et al.*, "Laser frequency combs for coherent optical communications," J. Lightwave Technol. **37**(7), 1663–1670 (2019).
4. N. Picqué and T. W. Hänsch, "Frequency comb spectroscopy," Nat. Photonics **13**(3), 146–157 (2019).
5. A. G. Griffith, R. K. W. Lau, J. Cardenas, *et al.*, "Silicon-chip mid-infrared frequency comb generation," Nat. Commun. **6**(1), 6299 (2015).
6. T. Udem, R. Holzwarth, and T. W. Hänsch, "Optical frequency metrology," Nature **416**(6877), 233–237 (2002).
7. C. Browning, H. H. Elwan, E. P. Martin, *et al.*, "Gain-switched optical frequency combs for future mobile radio-over-fiber millimeter-wave systems," J. Lightwave Technol. **36**(19), 4602–4610 (2018).
8. I. Coddington, N. Newbury, and W. Swann, "Dual-comb spectroscopy," Optica **3**(4), 414–426 (2016).
9. Y. Sugiyama, T. Kashimura, K. Kashimoto, *et al.*, "Precision dual-comb spectroscopy using wavelength-converted frequency combs with low repetition rates," Sci. Rep. **13**(1), 2549 (2023).
10. A. Muraviev, D. Konnov, S. Vasilyev, *et al.*, "Dual-frequency-comb uv spectroscopy with one million resolved comb lines," Optica **11**(11), 1486–1489 (2024).
11. I. Coddington, W. C. Swann, and N. R. Newbury, "Coherent multiheterodyne spectroscopy using stabilized optical frequency combs," Phys. Rev. Lett. **100**(1), 013902 (2008).
12. M. Soriano-Amat, M. A. Soto, V. Duran, *et al.*, "Common-path dual-comb spectroscopy using a single electro-optic modulator," J. Lightwave Technol. **38**(18), 5107–5115 (2020).
13. J. Mateu-Comas, A. Romero-Barrueco, M. Gonzalez-Herraez, *et al.*, "Phase-sensitive common-path dual frequency comb spectroscopy," in *29th International Conference on Optical Fiber Sensors*, vol. 13639 (SPIE, 2025), p. 136396C.
14. T. Ideguchi, A. Poisson, G. Guelachvili, *et al.*, "Adaptive real-time dual-comb spectroscopy," Nat. Commun. **5**(1), 3375 (2014).
15. A. M. Zolot, F. R. Giorgetta, E. Baumann, *et al.*, "Direct-comb molecular spectroscopy with accurate, resolved comb teeth over 43 thz," Opt. Lett. **37**(4), 638–640 (2012).
16. R. Liao, H. Tian, W. Liu, *et al.*, "Dual-comb generation from a single laser source: principles and spectroscopic applications towards mid-IR—A review," J. Physics: Photonics **2**(4), 042006 (2020).
17. G. Villares, A. Hugi, S. Blaser, *et al.*, "Dual-comb spectroscopy based on quantum-cascade-laser frequency combs," Nat. Commun. **5**(1), 5192 (2014).
18. M. Yu, Y. Okawachi, A. G. Griffith, *et al.*, "Silicon-chip-based mid-infrared dual-comb spectroscopy," Nat. Commun. **9**(1), 1869 (2018).
19. N. J. Lambert, L. S. Trainor, and H. G. L. Schwefel, "Microresonator-based electro-optic dual frequency comb," Commun. Phys. **6**(1), 89 (2023).
20. G. Millot, S. Pitois, M. Yan, *et al.*, "Frequency-agile dual-comb spectroscopy," Nat. Photonics **10**(1), 27–30 (2016).
21. P. M. Anandarajah, S. P. Ó Dúill, R. Zhou, *et al.*, "Enhanced optical comb generation by gain-switching a single-mode semiconductor laser close to its relaxation oscillation frequency," IEEE J. Sel. Top. Quantum Electron. **21**(6), 592–600 (2015).
22. P. M. Anandarajah, R. Maher, Y. Q. Xu, *et al.*, "Generation of coherent multicarrier signals by gain switching of discrete mode lasers," IEEE Photonics J. **3**(1), 112–122 (2011).
23. J. McCarthy and F. H. Peters, "On-chip gain switched frequency comb generation using a two sectioned single cavity laser without additional optical injection," Opt. Express **31**(18), 29619–29626 (2023).
24. T. Fortier and E. Baumann, "20 years of developments in optical frequency comb technology and applications," Commun. Phys. **2**(1), 153 (2019).
25. B. Jerez, P. Martín-Mateos, E. Prior, *et al.*, "Dual optical frequency comb architecture with capabilities from visible to mid-infrared," Opt. Express **24**(13), 14986–14994 (2016).

Optics EXPRESS

26. C. Quevedo-Galán, V. Durán, A. Rosado, *et al.*, "Gain-switched semiconductor lasers with pulsed excitation and optical injection for dual-comb spectroscopy," Opt. Express **28**(22), 33307–33317 (2020).
27. E. Russell, B. Corbett, and F. C. G. Gunning, "Gain-switched dual frequency comb at 2 μm," Opt. Express **30**(4), 5213–5221 (2022).
28. J. K. Alexander, L. Caro, M. Dernaika, *et al.*, "Integrated dual optical frequency comb source," Opt. Express **28**(11), 16900–16906 (2020).
29. T. Bunel, D. Chatterjee, J. Lumeau, *et al.*, "Dual-frequency comb in fiber fabry-perot resonator," APL Photonics **10**(3), 036115 (2025).
30. L. Ling, W. Lin, Z. Liang, *et al.*, "Practical ghz single-cavity all-fiber dual-comb laser for high-speed spectroscopy," Light. Sci. & Appl. **14**(1), 133 (2025).
31. S. M. Link, D. J. H. C. Maas, D. Waldburger, *et al.*, "Dual-comb spectroscopy of water vapor with a free-running semiconductor disk laser," Science **356**(6343), 1164–1168 (2017).
32. M. M. Krstić, J. V. Crnjanski, M. Ž. Banović, *et al.*, "Generation of a dual optical frequency comb by large signal modulation of a semiconductor laser," Opt. Lett. **46**(19), 4920–4923 (2021).
33. A. Delmade, M. Krstić, C. Browning, *et al.*, "Power efficient optical frequency comb generation using laser gain switching and dual-drive mach-zehnder modulator," Opt. Express **27**(17), 24135–24146 (2019).
34. L. A. Coldren, S. W. Corzine, and M. Mashanovitch, *Diode lasers and photonic integrated circuits* (Wiley, 2012), 2nd ed.
35. G. L. Lippi, J. Mørk, and G. P. Puccioni, "Numerical solutions to the laser rate equations with noise: technical issues, implementation and pitfalls," in *Nanophotonics VII* vol. 10672 (SPIE 2018).
36. M. M. Krstić, J. V. Crnjanski, and D. M. Gvozdić, "Injection power and detuning-dependent bistability in fabry-perot laser diodes," IEEE J. Sel. Top. Quantum Electron. **18**(2), 826–833 (2012).
37. A. E. Shitikov, V. E. Lobanov, N. M. Kondratiev, *et al.*, "Self-injection locking of a gain-switched laser diode," Phys. Rev. Appl. **15**(6), 064066 (2021).